

Engineering the Enolase Magnesium II Binding Site: Implications for Its Evolution[‡]

Bettina Schreier and Birte Höcker*

Max Planck Institute for Developmental Biology, Spemannstrasse 35, 72076 Tübingen, Germany

Received June 14, 2010; Revised Manuscript Received August 6, 2010

ABSTRACT: The glycolytic enzyme enolase catalyzes the reversible elimination of water from 2-phosphoglycerate (2-PGA) to form phosphoenolpyruvate (PEP). Two magnesium ions in the active site are thought to facilitate the reaction by activation of the C2 proton of 2-PGA and charge stabilization of the intermediate. The initial abstraction of a proton from a carboxylic acid is common to all members of the enolase superfamily, yet in all other known members of this superfamily, only one magnesium ion (MgI) per active site is sufficient to promote catalysis. We wanted to further investigate the importance of the second magnesium ion (MgII) for the catalytic mechanism of yeast enolase 1. Toward this end, we removed all MgII coordinating residues and replaced substrate–MgII interactions by introducing positively charged side chains. High-resolution crystal structures and activity assays show that the introduced positively charged side chains effectively prohibit MgII binding but fail to promote catalysis. We conclude that enolase is inactive without MgII, yet control mutants without additional positively charged side chains retain basal enolase activity through binding of magnesium to 2-PGA in an open active site without the help of MgII coordinating residues. Thus, we believe that ancestral enolase activity might have evolved in a member of the enolase superfamily that provides only the necessary catalytic residues and the binding site for MgI. Additionally, precatalytic binding of 2-PGA to the apo state of enolase was observed.

Enolase, a central metabolic enzyme catalyzing the conversion of 2-phosphoglycerate (2-PGA)¹ to phosphoenolpyruvate (PEP) in the glycolytic pathway, is the most prominent member of the enolase superfamily. All members consist of a central modified TIM-barrel domain with $(\beta/\alpha)_7\beta$ -architecture containing the catalytic residues and an $\alpha+\beta$ lid domain that influences substrate specificity.

The structure of dimeric yeast enolase 1 has been studied extensively (1–4). Several flexible loops have been identified that move upon substrate binding, leading to different overall conformations observed in enolase crystal structures (Figure 1A). Wild-type enolase cocrystallized with magnesium, and the substrate or product adopts a completely closed state with the flexible active site loops 36–43 from the lid domain and 153–169 and 251–277 from the barrel domain all in closed conformations (1, 3, 4). The S39A mutant of enolase was crystallized in an open state with all loops in the open conformation (5). In wild-type enolase crystals soaked with substrate, a third overall state, the apo state, has been described: Loop 36–43 is very far removed from the active site, while both loops 153–169 and 251–277 are open (2). Enolase can form asymmetric dimers with the two subunits adopting different overall conformations (3, 4).

Members of the enolase superfamily share a common initial reaction step (Figure 1B), the abstraction of the α -proton of a

carboxylate substrate by a general base (6), lysine 345 in yeast enolase 1 (1, 7). The resulting enolic intermediate is stabilized by a conserved active site magnesium ion, MgI, that interacts with the intermediate's carboxylate group (Figure 1C). Enolase itself is the only member in which the reaction intermediate is coordinated by a second magnesium ion, MgII (Figure 1C). MgII interacts with one carboxylate oxygen and a phosphate group oxygen of the substrate 2-PGA. Serine 39 in loop 36–43 of the lid domain is the only residue that directly interacts with MgII. Two water molecules positioned by aspartate 321 complete the coordination sphere of MgII (1, 8). Both magnesium ions are thought to participate in the crucial first step of the enolase reaction, the ionization of 2-PGA to give the negatively charged enolic intermediate and the stabilization thereof (1, 5, 9, 10) (Figure 1B). In the second step of the enolase reaction, the general acid glutamate 211 facilitates the dissociation of the hydroxide leaving group to form PEP (1, 7).

The exact function of MgII in the enolase reaction remains puzzling. In the enolase superfamily, electrostatic interactions with metal ions are thought to lower the pK_a of the substrate's α -proton to facilitate the proton abstraction step (11, 12). The exceptionally high pK_a of the 2-PGA α -proton (13) might explain the presence of the second magnesium ion in enolase. However, enolase superfamily enzymes of the MR subgroup, the acid sugar dehydratases, catalyze the proton abstraction of similarly weakly acidic substrates (14) yet utilize only one magnesium ion.

We wanted to further investigate the importance of MgII for the enolase reaction by elucidating whether MgII can be replaced by positively charged side chains as an alternative means of substrate stabilization. To test our hypothesis, we created yeast enolase 1 point mutants by a combined rational and computational design approach. In all mutants, the MgII-coordinating residues, S39 and D321, were replaced to remove all direct and indirect protein–MgII interactions. Positively charged side chains were introduced into the active site pocket to position the charged atoms in close

*The atomic coordinates of enolase mutants have been deposited in the Protein Data Bank as entries 2xh7 (enolase D321A), 2xh2 (enolase S39N/D321A), 2xh4 (enolase S39A/D321A), 2xgz (enolase S39N/D321R), and 2xh0 (enolase S39N/Q167K/D321R).

[†]To whom correspondence should be addressed. Phone: +49-7071-601322. Fax: +49-7071-601308. E-mail: birte.hoecker@tuebingen.mpg.de.

Abbreviations: 2-PGA, 2-phosphoglycerate; PEP, phosphoenolpyruvate; LDH, lactate dehydrogenase; PYK, pyruvate kinase; NADH, nicotinamide adenine dinucleotide; wt, wild-type; NA, enolase S39N/D321A; AA, enolase S39A/D321A; NR, enolase S39N/D321R; NKR, enolase S39N/Q167K/D321A; NA(A), enolase S39N/D321A/K345A; AA(A), enolase S39A/D321A/K345A; PDB, Protein Data Bank.

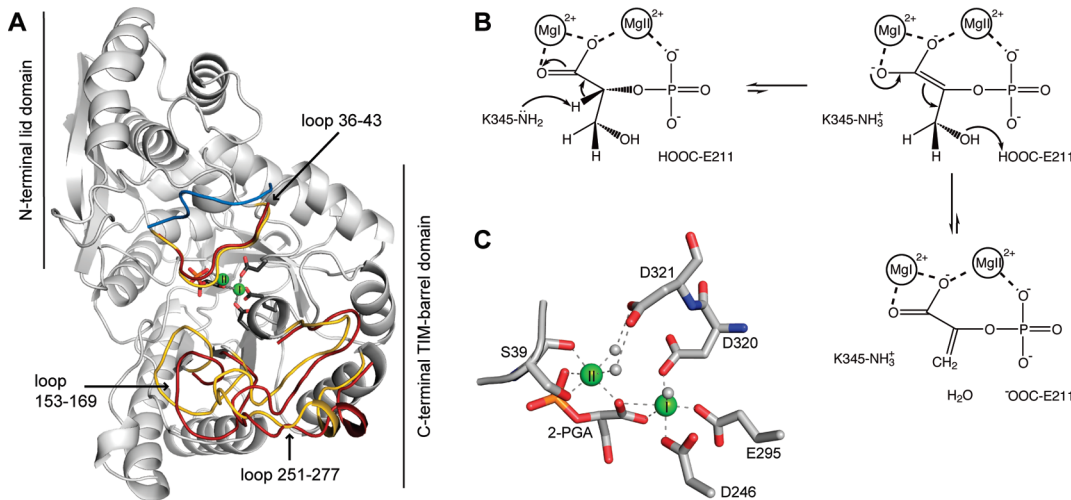


FIGURE 1: (A) Overall structure of wild-type enolase (PDB entry 1one) with flexible loops 36–43, 153–169, and 251–277 in closed conformations (yellow). MgI, MgII, 2-PGA, and the MgII-coordinating D246, E295, and D320 in the active site shown as spheres and sticks, respectively. To illustrate loop movements, flexible active site loops in open (red) and apo (blue) conformations are superimposed. (B) Schematic model of the enolase reaction mechanism, adapted from ref 4. (C) MgII coordination in the active site of wild-type enolase (PDB entry 1one). MgII (green sphere) interacts with 2-PGA, the side chain and backbone oxygen of S39, and two water molecules (gray spheres) positioned by D321.

proximity of 2-PGA, thus situated to substitute MgII interactions. Control mutants contained no additional positive charges interacting with the substrate.

To our surprise, while the mutants with the additional positively charged side chains are catalytically inactive, the control mutants retain enolase activity, albeit with a greatly reduced turnover rate compared to the that of wild-type. High-resolution crystal structures with bound ligand show that the positively charged side chains are positioned as predicted and thus effectively block MgII binding, yet they fail to promote catalysis. On the other hand, both high-resolution structural data and increased catalytic activity at high magnesium concentrations suggest that MgII still binds to the open active sites of the control mutants, thus enabling basal enolase activity. Our findings imply that enolase is not active without MgII bound to the substrate. Still, basal activity can be achieved in an open active site lacking the MgII coordinating residues because divalent metal ions from the solvent can be bound by the substrate alone.

Additionally, we determined a crystal structure that shows binding of 2-PGA to the active site of the apo state of enolase with unambiguous electron density. The position of the substrate in the active site and thus its interactions with the enzyme differ from those of the catalytic state, providing evidence of a precatalytic substrate-binding pocket.

EXPERIMENTAL PROCEDURES

Design of Enolase Mutants. Initial calculations using Dezymer (15) identified different rotamers of arginine and lysine at positions 321 and 167, respectively, with positively charged groups in contact with 2-PGA. Likewise, asparagine 39 was predicted to hydrogen bond with 2-PGA to promote loop closure of active site loop 36–43. These mutations were combined rationally in the NR (S39N/D321R) and NKR (S39N/Q167K/D321R) mutants. The control mutants NA (S39N/D321A) and AA (S39A/D321A) contained no additional positive charge (Figure S1 of the Supporting Information). Thus, the MgII interacting residues S39 and D321 were replaced in all mutants. Additionally, the D321A and S39A (5, 16) single mutants were analyzed to compare the effect of the single mutations with that of the double

mutations. To confirm that the measured activity is not due to contamination, the catalytic base K345 was mutated to alanine in the background of the NA and AA mutations, resulting in mutants NA(A) (S39N/D321A/K345A) and AA(A) (S39A/D321A/K345A).

Cloning of Enolase Expression Vectors. The wild-type enolase gene was amplified with PCR from genomic *Saccharomyces cerevisiae* DNA. Mutant enolase genes were constructed from the wild-type template with PCR site-directed mutagenesis. All resulting constructs were fully sequenced and contained no additional mutations. Wild-type and mutant genes were cloned into the pET-21a(+) expression vector.

Expression and Purification. Enolase wild-type and mutants were expressed as C-terminal 6x-His tag fusion proteins in *Escherichia coli* BL21; 1.5 L of LB medium in 3 L Erlenmeyer flasks was inoculated with a 10 mL overnight culture and grown to an OD₆₀₀ of 0.5–0.8. After induction with 1 mM IPTG, the flasks were shaken at 37 °C overnight. Cells were harvested by centrifugation and stored at –20 °C.

Cells were lysed by sonication in 50 mM Tris-HCl (pH 8.0), 300 mM KCl, 2 mM MgCl₂, and 20 mM imidazole. After removal of cell debris by centrifugation, a NiNTA column (Amersham Pharmacia HisTrap HP, 5 mL) was used for the first purification step. Initially, proteins were eluted with a linear imidazole gradient. For subsequent purifications, an optimized step elution protocol was developed, thus removing the need for concentrating the sample after this step. To remove imidazole, enolase-containing fractions were pooled and dialyzed against gel filtration buffer [20 mM Tris-HCl (pH 8.0), 2 mM MgCl₂, 0.5 mM EDTA, and 100 mM KCl]. To increase purity, an additional gel filtration step (GE Healthcare 26/60 Superdex 75 HiLoad) was performed. Enolase-containing fractions were pooled and dialyzed extensively against storage buffer [20 mM Tris-HCl (pH 8.0), 2 mM MgCl₂, and 0.5 mM EDTA]. Before activity assays were performed, an additional anion exchange step was conducted with conditions reported to efficiently bind possible trace levels of contamination of *E. coli* enolase (17). The resin (Sigma-Aldrich DEAE Sephadex) was extensively equilibrated with storage buffer. Enolase solutions were incubated with 20 mL of resin at 4 °C for 30 min. The supernatant containing the yeast enolase

Table 1: Statistics for the D321A, NA, AA, NR, and NKR Data Sets

| | D321A | NA | AA | NR | NKR |
|--|-----------------------|-----------------------|-----------------------|--------------------------|-----------------------|
| Data Collection ^a | | | | | |
| space group | <i>P</i> 1 | <i>P</i> 1 | <i>P</i> 1 | <i>P</i> 1 | <i>P</i> 1 |
| data range (Å) | 50.0–1.80 (1.91–1.80) | 40.0–1.79 (1.90–1.79) | 40.0–1.70 (1.80–1.70) | 40.0–1.80 (1.91–1.80) | 40.0–1.70 (1.80–1.70) |
| completeness (%) | 91.3 (89.6) | 93.1 (87.3) | 92.4 (91.1) | 75.9 (76.8) ^b | 93.0 (86.9) |
| <i>R</i> _{merge} (%) | 14.9 (68.2) | 12.6 (49.3) | 20.7 (82.7) | 16.1 (90.0) | 16.0 (77.1) |
| <i>I</i> / <i>σ</i> | 11.43 (3.12) | 12.74 (3.48) | 8.64 (2.65) | 11.66 (2.05) | 9.69 (2.34) |
| Wilson <i>B</i> value (Å ²) | 26.5 | 25.2 | 25.7 | 23.9 | 22.3 |
| Refinement | | | | | |
| <i>R</i> _{fact} (%) | 17.5 | 16.8 | 23.3 | 16.4 | 19.7 |
| <i>R</i> _{free} (%) | 21.4 | 20.9 | 27.9 | 20.8 | 24.6 |
| overall <i>B</i> value (Å ²) | 20.1 | 18.8 | 20.5 | 16.8 | 15.4 |

^aIn this section, the numbers in parentheses correspond to the values of the last shell. ^bThe NR data set contained ice rings; thus, certain resolution ranges had to be excluded from the calculations, resulting in a lower overall completeness.

was collected and sterile filtered. The purity of the proteins was checked by SDS-PAGE.

Crystallization. Protein crystals were obtained by standard vapor diffusion of 13–21 mg/mL purified enzyme in storage buffer against crystallization buffer containing different PEG's and salts at 20 °C (Table S1 of the Supporting Information). Enolase crystals belonging to space group *P*1 grew in 2–3 months. After being soaked in crystallization buffer with 3.5 mM 2-PGA or PEP and 3.5 mM MgCl₂ (if not present in the crystallization buffer) for a short time and transferred to a cryo solution with additional PEG 400, crystals were flash-frozen in liquid nitrogen. X-ray data of single crystals were collected with a MarCCD 225 mm detector at synchrotron beamline PXII (Swiss Light Source, Villigen PSI).

Structure Determination. Data were indexed and processed with XDS and converted with XDSConv (18). Molecular replacement searches were performed with Molrep from the CCP4 program suite (19) using the coordinates of wild-type enolase (PDB entry 2one) or a previously determined enolase mutant structure from this study as search models. Model building was performed in alternating rounds of computational refinement with REFMAC 5.4.0066 (20) and manual adjustments with Coot (21). Qualities of the final structures were judged by Molprobity (22) and WhatCheck (23). Data and refinement statistics for the different data sets are abbreviated in Table 1 and presented in more detail in Table S1 of the Supporting Information.

Structure Analysis. Structural superpositions were performed with the Pymol (24) align function.

Enolase Activity Assays. 2-PGA and NADH were purchased from Sigma. Coupling enzymes LDH and PYK were purchased from Roche. Na-ADP was purchased from Alexis. Activity in the conversion of 2-PGA to PEP was measured at 25 °C using a coupled assay with LDH and PYK. To start the reaction, 0.01 μM (wild-type), 5 μM (D321A and S39A), or 10 μM (other mutants) purified enzyme was added to a cuvette containing 1 mL of reaction mix [50 mM HEPES (pH 7.5), 45 μM NADH, 0.22 mM Na-ADP, 1.38 units/mL LDH, and 1.2 units/mL PYK] and either 2 mM MgCl₂ with a 2-PGA concentration ranging from 5 to 600 μM or 200 μM 2-PGA with a MgCl₂ concentration ranging from 0.03 to 25 mM. The decrease in absorption at 340 nm was monitored with a Varian Cary 50 Scan spectrophotometer. Initial reaction rates were determined from fits to the linear portion of the curves. Three measurements with independently

purified batches of protein were performed for each variant. Values for *k*_{cat} and *K*_M were determined from best fits of the Michaelis–Menten equation to the averaged data. The baseline was determined by monitoring the decrease in absorption after addition of water instead of enzyme, and the detection limit of the coupled assay was thereby calculated.

¹H Proton Exchange Measurements. This highly sensitive method of assaying the capacity of mutant enolases to exchange the C-2 proton of 2-PGA was adapted from ref 7. Assay solutions contained 25 mM Tris-DCl (pD 7.5), 2 mM MgCl₂, and 1 mM 2-PGA in D₂O. After a reference spectrum had been recorded, the reaction was started by addition of 0.02 μM wild-type or 0.5 μM mutant enzyme. One-dimensional NMR spectra were recorded on a 600 MHz Bruker Avance III spectrometer immediately and after incubation for 2 days at 25 °C. As a control, spectra of 2-PGA in assay solution were recorded without addition of enzyme.

RESULTS AND DISCUSSION

Crystal Structures. We obtained high-resolution crystal structures of D321A, NA, AA, NR, and NKR in complex with magnesium and 2-PGA or PEP (Table 1). Enolase mutants crystallized in this study adopt the closed, open, or apo state and align with root-mean-square deviations between 0.25 and 0.33 Å over all Cα atoms with previously published enolase structures in closed, open, and apo states (Figure S2 of the Supporting Information). Although enolase crystals were soaked with substrate, we observe the same loop conformations that were found in cocrystallization experiments. As the flexible loops are not involved in crystal contacts, the necessary loop movements can occur in the confines of a protein crystal.

Structures of Active Sites of Enolase Mutants. In all crystal structures determined in this study, unambiguous density for the ligands 2-PGA or PEP and MgI is present in the active site (Figure 2). While we observe binding of MgII to D321A and AA, it is absent in the other mutant structures. The overall conformation of the active site, the binding of the ligands 2-PGA, PEP, and MgI, and the conformation of the catalytic side chains K345 and E211 are not affected by the mutations. Thus, the observed activity loss appears to be a direct result of the loss of MgII binding and changes in active site closure.

The D321A mutant is crystallized in the closed state, with MgII bound and all flexible loops in the closed conformation

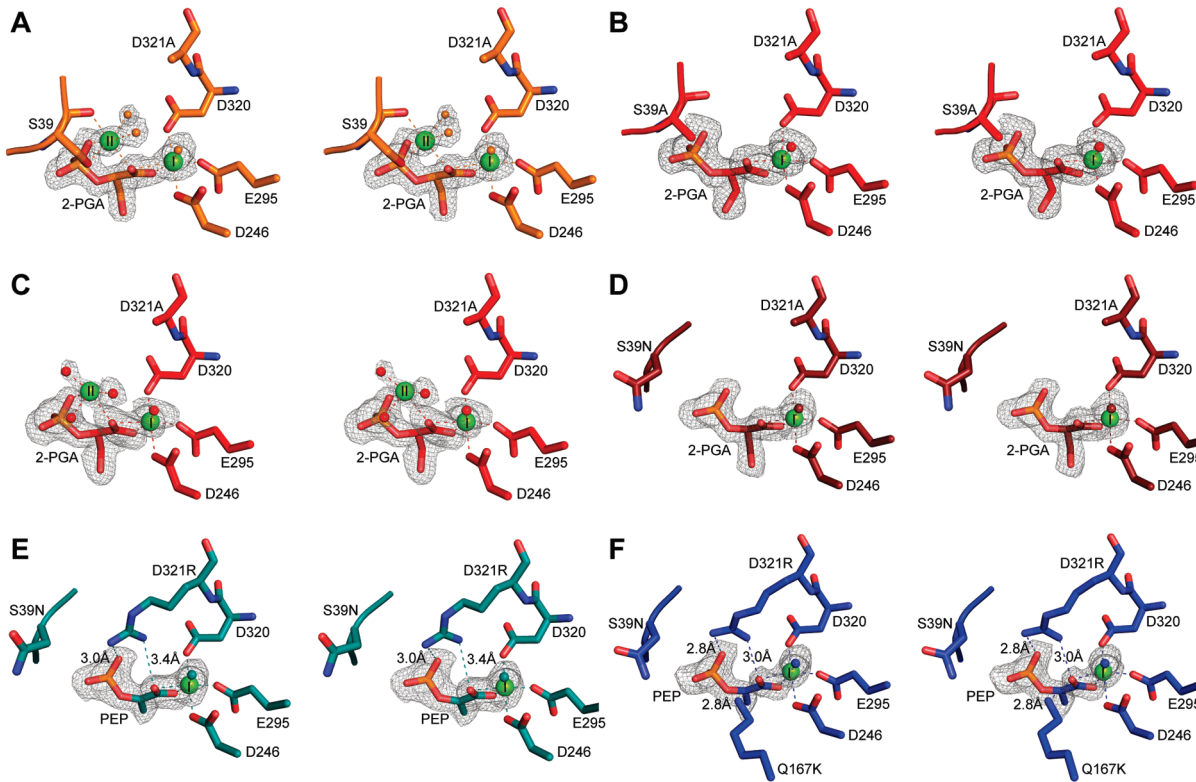


FIGURE 2: Stereo images of the active sites of enolase mutants. In all mutants, MgI and substrate binding as well as the conformation of the active site side chains is not affected by the mutations. The omit electron density ($F_o - F_c$) for the ligands is contoured at 2.0σ (B, C, and F) or 3.0σ (A, D, and E). Water molecules are shown as small spheres. (A) Active site of D321A with density for 2-PGA, MgI, and MgII. Both subunits adopt the closed state. MgII is bound in the wild-type position; only the positions of the two coordinating water molecules differ slightly from those of the wild-type. (B) Active site of AA subunit A. This subunit adopts the closed state. MgII is not bound to the active site. (C) Active site of AA subunit B. No density for loop 36–43 is present; thus, the active site of subunit B is accessible to the solvent. All other loops adopt the closed conformation. Density for MgII bound in the wild-type position and three coordinating water molecules is present. Bond lengths and angles exclude the possibility of a water cluster. (D) Active site of NA, subunit A. N39 does not hydrogen bond to 2-PGA as predicted, leaving loop 36–43 in the open conformation and the active site accessible to solvent. MgII is not bound to the active site. (E) Active site of NR, subunit A. N39 does not hydrogen bond to PEP as predicted, leaving loop 36–43 in the open conformation and the active site accessible to solvent. As predicted, R321 is in contact with PEP, thus blocking MgII binding. (F) Active site of NKR, subunit A. N39 does not hydrogen bond to PEP as predicted, leaving loop 36–43 in the open conformation and the active site accessible to solvent. Both R321 and K167 are in contact with PEP, thus blocking MgII binding.

(Figure 2A). As a result of the D321A mutation, the position of the two water molecules that complete the MgII coordination sphere differs slightly from that of the wild-type.

The subunit A of mutant AA adopts the completely closed state, although no MgII is bound to the active site (Figure 2B). In subunit B in the same crystal, no density for loop 36–43 is visible, indicating high loop flexibility. On the other hand, density for MgII and three of the four coordinating waters that would complete its hexagonal coordination sphere is clearly present (Figure 2C). The fact that the density for MgII is significantly lower than for MgI indicates that MgII is not present in all active sites of the crystal lattice. Still, this structure confirms that MgII can bind to 2-PGA in an open active site lacking any additional side chain interactions with the protein. 2-PGA binds divalent cations like magnesium in solution (25), which explains why the substrate in an open binding pocket is sufficient to bind magnesium with low affinity.

NA subunit A, NR subunit A, and NKR are crystallized in the open state without bound MgII (Figure 2D–F). No hydrogen bonds are formed between N39 and the substrate as predicted; instead, N39 points away from the active site, leaving loop 36–43 in an open conformation. In contrast, R321 and K167 interact with the substrate as predicted, although the rotamers found in the crystal structure differ from those of the predictions. Both R321 and K167 are calculated to be protonated by ProPKA (26, 27).

Thus, R321 and K167 sterically and electrostatically prohibit binding of MgII to NR and NKR. Only in the precatalytic apo structure of NR subunit B is R321 not in contact with the substrate (Figure S3 of the Supporting Information).

We observe MgII binding to the open state AA but not to the open state NA structure, which might be due to the lower magnesium concentrations in the NA crystallization buffer (Table S1 of the Supporting Information).

Binding of 2-PGA to Apo Enolase. The structures of NA and NR show that 2-PGA and PEP can bind to the so-called apo state of enolase (Figure 3 and Figure S3 of the Supporting Information). As the diameter of the active site in the apo state is approximately 1.5 Å wider than in the open or closed state, it is impossible to satisfy all ligand side chain interactions. In NA subunit B, 2-PGA is not bound directly to MgI but occupies its second coordination sphere. The first coordination sphere is completed by two additional water molecules in contact with both MgI and 2-PGA (Figure 3A). Thus, the three water molecules bound to MgI in substrate-free Mg^{2+} -bound enolase (28) are still present in the initial binding pocket and contribute to 2-PGA binding. As the position of 2-PGA is shifted, catalytic contacts with the catalytic base K345 and the catalytic acid E211 are not established, indicating that the observed initial binding mode is precatalytic. Instead, E211 is flexible while K345 hydrogen bonds to a carboxy group oxygen of 2-PGA.

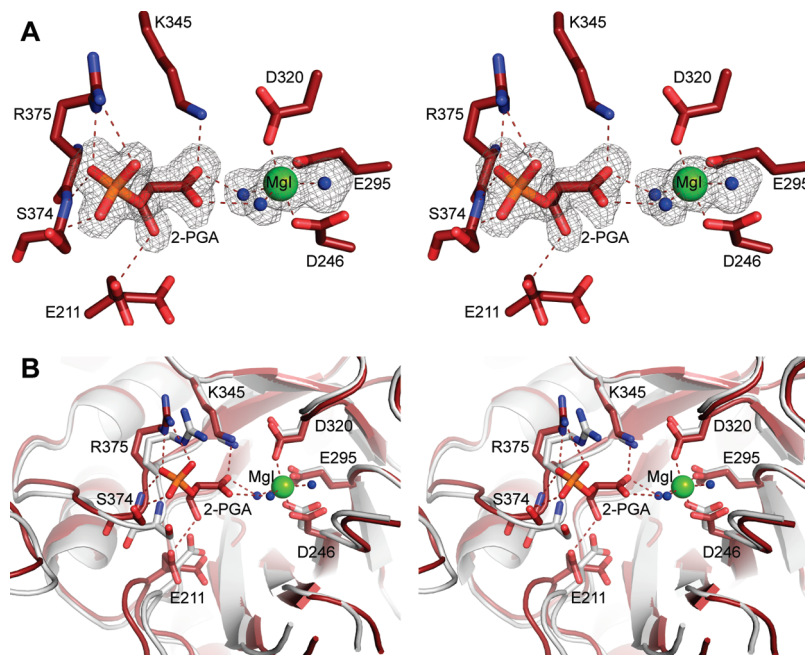


FIGURE 3: Stereo images illustrating binding of 2-PGA to the apo structure of enolase NA subunit B. (A) The omit electron density ($F_o - F_c$) for 2-PGA, MgI (green sphere), and the water molecules (blue spheres) is contoured at 3.0σ . 2-PGA hydrogen bonds to S374, R375, K345, and two water molecules in the first coordination sphere of MgI. Catalytic contacts of 2-PGA with K345 and E211 are not established. (B) Superimposition of enolase NA subunit B (dark red) with wild-type enolase in the closed state (gray, PDB entry 1one). 2-PGA, MgI (green sphere), and additional water molecules (blue spheres) are shown in NA subunit B. Alignment was achieved only with the β -sheet residues of both molecules (residues 151–155, 168–172, 242–246, 293–295, 316–318, 341–344, 368–371, and 394–396; resulting root-mean-square deviation of 0.64 over all atoms) to illustrate loop movements. The largest movements occur in loop 372–381 containing R375 (distance between C α atoms in the apo and closed conformation of 1.0 \AA) and S374 (distance between C α atoms in the apo and closed conformation of 1.6 \AA) and in the loop containing catalytic acid E211 (distance between C α atoms in the apo and closed conformation of 1.2 \AA).

The superimposition of enolase NA subunit B in the apo state with wild-type enolase in the closed state illustrates the movements necessary to switch between conformations (Figure 3B). The largest displacements are observed for residues S374 and R375 and catalytic base E211. Thus, we presume that initial binding of the substrate to the apo structure initiates structural rearrangements. Foremost, movement of the loops containing S374, R375, and E211 is necessary to reduce the diameter of the active site pocket and establish catalytic contacts between the substrate and MgI, K345, and E211. Subsequently, MgII is bound followed by closure of loops 36–43, 153–169, and 250–277 (1–3). The crystal structure of enolase E211Q [PDB entry 1p48 (29)] shows loop 153–169 in an intermediate position between the opened and fully closed state, while loop 36–43 is already fully closed, suggesting that movement of loop 36–43 precedes that of loop 153–169. Only then is the active site fully closed and can efficient catalysis occur.

Substrate binding has been observed in apo state crystals of wild-type enolase as well (2), yet the poor electron density for the substrate led to misinterpretation of the substrate backbone conformation [PDB entry 7enl (2)]. In the case of NA subunit B, the electron density for 2-PGA, MgI, and all active site waters is very well-defined (Figure 3A). In the mutant NR, PEP also binds to the apo state. However, the electron density for the ligand is poor and the conformation shown might be ambiguous (Figure S3 of the Supporting Information).

Catalytic Activity of Enolase Mutants. The catalytic activities in the conversion of 2-PGA to PEP were determined for enolase wild-type and mutants (Figure 4). Kinetic parameters for wild-type enolase are in good accordance with previously published data (4, 5, 7); the k_{cat} of the S39A mutant is in reasonable

accordance with the one determined by Poyner et al. (5) (Table 2). Kinetic parameters for S39A determined by Brewer et al. (16) differ from the results of this study. It is possible that their purifications retained traces of isoenzyme enolase 2.

While the D321A mutant is 10^3 -fold less active than the wild-type, it retains approximately 15 times more activity than the S39A mutant (Figure 4A). As serine 39 directly interacts with MgII whereas aspartate 321 only functions in positioning two water molecules as interaction partners, it is reasonable to conclude that serine 39 is more important for MgII binding than aspartate 321, resulting in a greater activity loss in the S39A mutant. Mutants with additional positively charged side chains, NR and NKR, are catalytically inactive. In contrast, the control mutants NA and AA retain enolase activity (Figure 4B), yet NA and AA are 10^5 -fold less active than the wild-type (Table 2).

When the catalytic base K345 of NA and AA is mutated to alanine, this basal activity is completely lost (Figure 4B,D), indicating that the observed activity of NA and AA is not an artifact or due to contamination with wild-type *E. coli* enolase. Traces of *E. coli* enolase or yeast enolase 2 are easily copurified with enolase 1, which might explain why previous studies could determine catalytic parameters for enolase K345E, albeit at very low levels (4, 7). However, after purification by Ni affinity chromatography and gel filtration, we performed an additional anion exchange step with conditions reported to efficiently bind possible trace levels of contamination of *E. coli* enolase (17). Catalytic parameters of *E. coli* enolase are very similar to those of yeast enolase 1, with an optimum around 2 mM Mg^{2+} (17). Thus, the fact that the activity of enolase NA and AA is activated by high magnesium concentrations but not inhibited like that of wild-type yeast or *E. coli* enolase, along with the purifications of

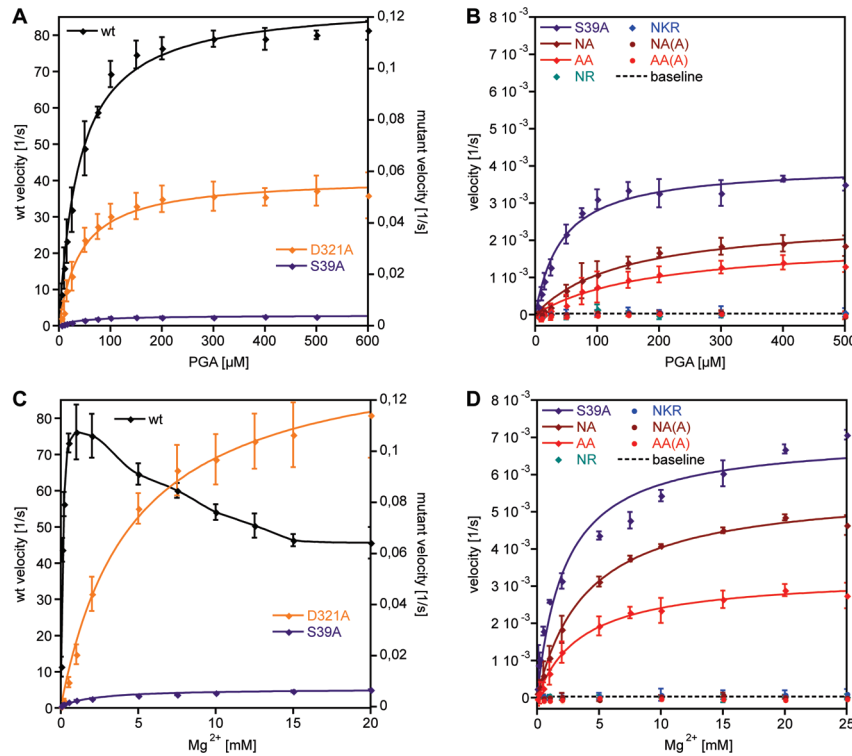


FIGURE 4: Catalytic activities of enolase wild-type and mutants. Plotted are the mean and standard deviation calculated from three independent measurements of three batches of purified enzyme for each mutant along with the Michaelis–Menten (A and B) or hyperbolic (C and D) best fit to that data. (A) Catalytic activities in the conversion of 2-PGA to PEP of wild-type enolase, D321A, and S39A in the presence of 2 mM Mg²⁺. (B) Catalytic activity in the conversion of 2-PGA to PEP of enolase mutants in the presence of 2 mM Mg²⁺. (C) Influence of the magnesium concentration on catalytic activities of wild-type enolase, D321A, and S39A with 200 μM 2-PGA. (D) Influence of the magnesium concentration on catalytic activities of enolase mutants with 200 μM 2-PGA.

Table 2: Kinetic Parameters for Enolase Wild-Type and Mutants

| | | k_{cat} (s ⁻¹) | K_M (μM 2-PGA) | k_{cat}/K_M (M ⁻¹ s ⁻¹) | $V_{1/2}$ (mM Mg ²⁺) |
|-------|------------------|-------------------------------------|------------------|---|----------------------------------|
| wt | — | 89 ± 2 | 39 ± 3 | 2.3×10^6 | — |
| D321A | D321A | 0.058 ± 0.002 | 43 ± 6 | 1.3×10^3 | 4.6 ± 0.5 |
| S39A | S39A | 0.0040 ± 0.0002 | 44 ± 6 | 91.7 | 2.3 ± 0.5 |
| NA | S39N/D321A | 0.0026 ± 0.0002 | 144 ± 26 | 18.1 | 4.0 ± 0.3 |
| AA | S39A/D321A | 0.0020 ± 0.0002 | 194 ± 52 | 10.3 | 3.7 ± 0.3 |
| NR | S39N/D321R | $< 2.8 \times 10^{-5}^a$ | — | — | — |
| NKR | S39N/Q167K/D321R | $< 2.8 \times 10^{-5}^a$ | — | — | — |
| NA(A) | S39N/D321A/K345A | $< 2.8 \times 10^{-5}^a$ | — | — | — |
| AA(A) | S39A/D321A/K345A | $< 2.8 \times 10^{-5}^a$ | — | — | — |

^aThe catalytic activity of the mutants NR, NKR, NA(A), and AA(A) is below the detection limit ($< 2.8 \times 10^{-5}$) of the coupled assay.

the mutants NR, NKR, NA(A) and AA(A) that completely lack enolase activity, clearly speaks against contamination of our purifications with *E. coli* enolase.

The K_M for 2-PGA of S39A and D321A is not affected by the introduced mutations, whereas the K_M for 2-PGA of the double mutants NA and AA is slightly increased (Table 2).

Influence of Magnesium Concentrations on Activity. High magnesium concentrations strongly affect the activity of enolase wild-type and mutants. The catalytic activity of wild-type enolase reaches its maximum at magnesium concentrations between 1 and 2 mM and is inhibited at higher concentrations (Figure 4C), as described previously (30, 31). In the ordered kinetic mechanism of enolase, MgII release precedes product release; thus, high Mg²⁺ concentrations limit the reaction rate due to slower release of MgII (31). In contrast, D321A, S39A, NA, and AA are activated by high magnesium concentrations

(Figure 4C,D). The apparent activation constant for MgII $V_{1/2}$ (Table 2) lies in the same range for D321A, NA, and AA. The hyperbolic fit to the S39A data fits less well, making it difficult to interpret the value for $V_{1/2}$. This effect has been described previously for S39A (5). The mutations reduce the affinity for MgII, and the thus accelerated MgII release is no longer rate-limiting, resulting in the observed activation profile.

NA is significantly more active than AA, especially at magnesium concentrations of > 2 mM. Increasing the concentration of Mg²⁺ has no effect on the catalytically inactive mutants NR, NKR, NA(A), and AA(A).

¹H Proton Exchange Measurements. To confirm the results of the activity assays, the capacity to exchange the C-2 proton of 2-PGA was analyzed by NMR (Figure S4 of the Supporting Information). As expected, in samples containing wild-type enolase the 2-PGA proton peaks were diminished over

time while a new peak for the PEP proton appeared (Figure S4A of the Supporting Information). No change in the spectra could be detected in samples containing NKR after incubation at 25 °C for 2 days (Figure S4B of the Supporting Information). This confirms that NKR is indeed completely inactive and not simply below the detection limit of the coupled assay. Additionally, our analysis shows that no uncatalyzed conversion of 2-PGA to PEP is detectable under the same conditions.

Concluding Remarks. Both structures and activity assays confirm that the introduced side chains R321 and K167 in NR and NKR effectively inhibit MgII binding both sterically and electrostatically. Both R321 and K167 are in close contact with the substrate and predicted to be protonated by ProPKA (26, 27), yet slight variations between subunits of one crystal of both bond distances and angles of the side chain–substrate interactions indicate some flexibility in the positioning of R321 and K167. Thus, one explanation for R321 and K167's failure to promote catalysis could be the imperfect geometry of the interactions with the substrate. It seems that either the charge introduced by the side chains is insufficient for charge stabilization and substrate activation or charged side chains are simply not structurally appropriate for that task in the enolase active site. We conclude that MgII is essential for enolase activity and cannot be replaced by the introduced positively charged side chains.

So how is MgII binding impaired, and what is the resulting effect on activity? The crystal structures indicate that rather than incorrect coordination there is a weakening of MgII binding through reduced occupancy. The increase in magnesium concentration does improve the turnover in all active mutants significantly, but not close to wild-type levels. A second intermingled factor is a change in active site accessibility. Loop 36–43 efficiently closes the active site pocket in the wild-type interacting solely with MgII via the side chain and backbone of residue S39. The S39A mutation impairs MgII binding but still allows the loop to close as observed in the AA mutant, while mutants with the S39N mutation (NA, NR, and NKR) do not adopt the fully close state in our crystal structures. Although shielding from solvent often improves catalysis, the greater accessibility enables NA to be more easily activated by increasing magnesium concentrations than AA. Thus, the loss of affinity for MgII affects activity more severely than impaired loop closure.

Evolutionary Perspective. The active sites of NA and AA remain accessible to solvent (Figure 2B–D), making it possible for magnesium to directly bind to the substrate (Figure 2C) and thus promote catalysis. We therefore believe that ancestral enolase activity might have evolved in a member of the enolase superfamily that lacks the MgII binding site but provides the necessary catalytic residues. Our results show that binding of magnesium to the substrate in an open active site pocket is sufficient for basal levels of enolase activity. It is reasonable to conclude that other divalent ions would likewise promote activity, as wild-type enolase was shown to be active with a wide range of divalent metal cofactors (31). Taking into account the fact that the uncatalyzed conversion of 2-PGA to PEP is too slow to be measured by NMR, the basal enolase activity that can be thus achieved is enough to provide an evolutionary advantage.

ACKNOWLEDGMENT

We thank Dr. Remco Sprangers for collection of NMR data and help with its interpretation, Sooruban Shanmugaratnam for technical assistance, and Dr. Reinhard Sternner for comments on the manuscript.

SUPPORTING INFORMATION AVAILABLE

Predicted active site structures of the designed enolase mutants, superimpositions of enolase wild-type and mutants in closed, open, and apo conformation, binding of PEP to the apo structure of enolase NR, ¹H proton exchange measurements, and detailed crystallographic data and refinement statistics. This material is available free of charge via the Internet at <http://pubs.acs.org>.

REFERENCES

- Larsen, T. M., Wedekind, J. E., Rayment, I., and Reed, G. H. (1996) A carboxylate oxygen of the substrate bridges the magnesium ions at the active site of enolase: Structure of the yeast enzyme complexed with the equilibrium mixture of 2-phosphoglycerate and phosphoenolpyruvate at 1.8 Å resolution. *Biochemistry* 35, 4349–4358.
- Lebioda, L., Stec, B., Brewer, J. M., and Tykarska, E. (1991) Inhibition of enolase: The crystal structures of enolase-Ca²⁺-2-phosphoglycerate and enolase-Zn²⁺-phosphoglycolate complexes at 2.2-Å resolution. *Biochemistry* 30, 2823–2827.
- Zhang, E., Brewer, J. M., Minor, W., Carreira, L. A., and Lebioda, L. (1997) Mechanism of enolase: The crystal structure of asymmetric dimer enolase-2-phospho-D-glycerate/enolase-phosphoenolpyruvate at 2.0 Å resolution. *Biochemistry* 36, 12526–12534.
- Sims, P. A., Menefee, A. L., Larsen, T. M., Mansoorabadi, S. O., and Reed, G. H. (2006) Structure and catalytic properties of an engineered heterodimer of enolase composed of one active and one inactive subunit. *J. Mol. Biol.* 355, 422–431.
- Poyner, R. R., Larsen, T. M., Wong, S. W., and Reed, G. H. (2002) Functional and structural changes due to a serine to alanine mutation in the active-site flap of enolase. *Arch. Biochem. Biophys.* 401, 155–163.
- Babbitt, P. C., Hasson, M. S., Wedekind, J. E., Palmer, D. R., Barrett, W. C., Reed, G. H., Rayment, I., Ringe, D., Kenyon, G. L., and Gerlt, J. A. (1996) The enolase superfamily: A general strategy for enzyme-catalyzed abstraction of the α-protons of carboxylic acids. *Biochemistry* 35, 16489–16501.
- Poyner, R. R., Laughlin, L. T., Sowa, G. A., and Reed, G. H. (1996) Toward identification of acid/base catalysts in the active site of enolase: Comparison of the properties of K345A, E168Q, and E211Q variants. *Biochemistry* 35, 1692–1699.
- Zhang, E., Hatada, M., Brewer, J. M., and Lebioda, L. (1994) Catalytic metal ion binding in enolase: The crystal structure of an enolase-Mn²⁺-phosphonoacetohydroxamate complex at 2.4-Å resolution. *Biochemistry* 33, 6295–6300.
- Wedekind, J. E., Poyner, R. R., Reed, G. H., and Rayment, I. (1994) Chelation of serine 39 to Mg²⁺ latches a gate at the active site of enolase: Structure of the bis(Mg²⁺) complex of yeast enolase and the intermediate analog phosphonoacetohydroxamate at 2.1-Å resolution. *Biochemistry* 33, 9333–9342.
- Liu, H. Y., Zhang, Y. K., and Yang, W. T. (2000) How is the active site of enolase organized to catalyze two different reaction steps? *J. Am. Chem. Soc.* 122, 6560–6570.
- Gerlt, J. A., and Gassman, P. G. (1992) Understanding Enzyme-Catalyzed Proton Abstraction from Carbon Acids: Details of Stepwise Mechanisms for β-Elimination Reactions. *J. Am. Chem. Soc.* 114, 5928–5934.
- Guthrie, J. P., and Kluger, R. (1993) Electrostatic Stabilization Can Explain the Unexpected Acidity of Carbon Acids in Enzyme-Catalyzed Reactions. *J. Am. Chem. Soc.* 115, 11569–11572.
- Hilal, S. H., Brewer, J. M., Lebioda, L., and Carreira, L. A. (1995) Calculated effects of the chemical environment of 2-phospho-D-glycerate on the pK_a of its carbon-2 and correlations with the proposed mechanism of action of enolase. *Biochem. Biophys. Res. Commun.* 211, 607–613.
- Rakus, J. F., Fedorov, A. A., Fedorov, E. V., Glasner, M. E., Vick, J. E., Babbitt, P. C., Almo, S. C., and Gerlt, J. A. (2007) Evolution of enzymatic activities in the enolase superfamily: D-Mannose dehydratase from *Novosphingobium aromaticivorans*. *Biochemistry* 46, 12896–12908.
- Looger, L. L., and Hellinga, H. W. (2001) Generalized dead-end elimination algorithms make large-scale protein side chain structure prediction tractable: Implications for protein design and structural genomics. *J. Mol. Biol.* 307, 429–445.
- Brewer, J. M., Glover, C. V., Holland, M. J., and Lebioda, L. (1998) Significance of the enzymatic properties of yeast S39A enolase to the catalytic mechanism. *Biochim. Biophys. Acta* 1383, 351–355.

17. Spring, T. G., and Wold, F. (1971) The Purification and Characterization of *Escherichia coli* Enolase. *J. Biol. Chem.* **246**, 6797–6802.
18. Kabsch, W. (1988) Automatic-Indexing of Rotation Diffraction Patterns. *J. Appl. Crystallogr.* **21**, 67–71.
19. Collaborative Computational Project Number 4 (1994) The CCP4 suite: Programs for protein crystallography. *Acta Crystallogr. D50*, 760–763.
20. Murshudov, G. N., Vagin, A. A., and Dodson, E. J. (1997) Refinement of macromolecular structures by the maximum-likelihood method. *Acta Crystallogr. D53*, 240–255.
21. Emsley, P., and Cowtan, K. (2004) Coot: Model-building tools for molecular graphics. *Acta Crystallogr. D60*, 2126–2132.
22. Davis, I. W., Leaver-Fay, A., Chen, V. B., Block, J. N., Kapral, G. J., Wang, X., Murray, L. W., Arendall, W. B., III, Snoeyink, J., Richardson, J. S., and Richardson, D. C. (2007) MolProbity: All-atom contacts and structure validation for proteins and nucleic acids. *Nucleic Acids Res.* **35**, W375–W383.
23. Hooft, R. W., Vriend, G., Sander, C., and Abola, E. E. (1996) Errors in protein structures. *Nature* **381**, 272.
24. DeLano, W. L. (2002) The PyMOL Molecular Graphics System, DeLano Scientific, Palo Alto, CA.
25. Wold, F., and Ballou, C. E. (1957) Studies on the enzyme enolase. I. Equilibrium studies. *J. Biol. Chem.* **227**, 301–312.
26. Li, H., Robertson, A. D., and Jensen, J. H. (2005) Very fast empirical prediction and rationalization of protein pK_a values. *Proteins* **61**, 704–721.
27. Bas, D. C., Rogers, D. M., and Jensen, J. H. (2008) Very fast prediction and rationalization of pK_a values for protein-ligand complexes. *Proteins* **73**, 765–783.
28. Wedekind, J. E., Reed, G. H., and Rayment, I. (1995) Octahedral coordination at the high-affinity metal site in enolase: Crystallographic analysis of the MgII–enzyme complex from yeast at 1.9 Å resolution. *Biochemistry* **34**, 4325–4330.
29. Sims, P. A., Larsen, T. M., Poyner, R. R., Cleland, W. W., and Reed, G. H. (2003) Reverse protonation is the key to general acid-base catalysis in enolase. *Biochemistry* **42**, 8298–8306.
30. Faller, L. D., Baroudy, B. M., Johnson, A. M., and Ewall, R. X. (1977) Magnesium ion requirements for yeast enolase activity. *Biochemistry* **16**, 3864–3869.
31. Poyner, R. R., Cleland, W. W., and Reed, G. H. (2001) Role of metal ions in catalysis by enolase: An ordered kinetic mechanism for a single substrate enzyme. *Biochemistry* **40**, 8009–8017.